International Journal of Heat and Mass Transfer 52 (2009) 2362–2369

Contents lists available at ScienceDirect

International Journal of Heat and Mass Transfer

journal homepage: www.elsevier.com/locate/ijhmt

Constructal steam generator architecture

Yong Sung Kim [a,c], Sylvie Lorente [b], Adrian Bejan [c,*]

[a] Doosan Heavy Industries & Construction, 555 Gwigok-Dong, Changwon, Gyeongnam 641-792, South Korea
[b] University of Toulouse, INSA, Laboratory of Materials and Durability of Constructions, 135 Avenue de Rangueil, 31077 Toulouse, France
[c] Duke University, Department of Mechanical Engineering and Materials Science, Durham, NC 27708-0300, USA

ARTICLE INFO

Article history:
Received 16 September 2008
Received in revised form 10 October 2008
Available online 5 February 2009

Keywords:
Constructal
Steam generator
Steam power plant
Design as science
Scaling up
Size effect
Morphing

ABSTRACT

This paper shows that the architecture of a steam generator for a power plant can be deduced on the basis of the constructal law. According to constructal theory, the flow architecture emerges in time such that it provides progressively greater access to its currents. The circulation of water is driven by buoyancy in one large tube (the downcomer) and many parallel smaller tubes (the riser). The total flow volume is fixed. Two flow models are used: single phase liquid in the downcomer and riser, and liquid–vapor mixture in the riser tubes. Features that result from constructal design are: the tube diameters, the number of riser tubes, the water circulation rate, the rate of steam production, and how the flow architecture should change when the operating pressure and the size of the flow system change.

1. Introduction

In this paper we propose to use constructal theory in the conceptual design of steam generators for large-scale commercial power plants. Steam generators represent a major area for engineering development, and a most fertile field for novel methods of design and for new design concepts. Constructal theory is ideally suited for this because it begins the conceptual design with a clean slate, and invites the designer to recognize and consider all the possible and competing configurations. The architecture of the complex flow system is the unknown. There is no bias, no pre-existing rule of thumb.

Constructal theory focuses attention on the generation of flow configurations [1,2]. Natural and engineered flow systems have configurations. They are not amorphous. "Flow" represents the movement of one entity relative to another (the background). To describe a flow, we speak of what the flow carries (fluid, heat, mass), how much it carries (mass flow rate, heat current, species flow rate), and where the stream is located in the available space. The "where" is the drawing, i.e. the design.

According to constructal theory, the generation of flow configuration can be reasoned based on an *evolutionary* principle of increase of flow access in time (the constructal law): "For a finite-size flow system to persist in time (to live) its configuration must change in time such that it provides greater and greater access to its currents" [3]. The evolution of flow configuration is like an animated movie, which runs in a particular direction in time such that each screen (i.e. each drawing) is replaced by a screen that flows more easily *as a whole*.

The flow configuration that emerges from this natural tendency is the result of the persistent struggle, contortion and mechanism by which the global flow system achieves global flow performance under global constraints. A growing literature is showing that the constructal law is being used for better engineering and for better organization of the movement and connecting of people, goods and information [1–18]. This direction is recognized as *constructal design*, and with it designers seek not only better configurations but also better (faster, cheaper, more direct, more reliable) strategies for generating the geometry that is missing.

The global objective of a steam generator is to heat the stream of water in the most compact manner possible [19,20]. Compactness translates ultimately into less volume, weight and cost of manufacturing, transportation, assembly and maintenance. It is also related to the improvement of thermodynamic performance subject to finite-size constraints, as we discuss further in Section 6. Here we account for this complex design mission by fixing the volume of the flow device, and by using this constraint consistently at every level of construction, i.e., at every length scale.

The water flow through the steam generator is driven by the self-pumping principle illustrated in Fig. 1. The vertical tubes shown on the right are heated, bubbles form in them, and the liquid-steam mixture flows upward. Together, they constitute the "riser", which is heated by external combustion gases.

* Corresponding author. Tel.: +1 919 660 5309; fax: +1 919 660 8963.
E-mail address: abejan@duke.edu (A. Bejan).

0017-9310/$ - see front matter © 2008 Elsevier Ltd. All rights reserved.
doi:10.1016/j.ijheatmasstransfer.2008.10.021

Nomenclature

A	area, m^2
b	constants
$B_{1,2}$	constant
$c_{1,2}$	constants
c_P	specific heat at constant pressure, J kg^{-1} K^{-1}
D	column diameter, m
f	friction factor
g	gravitational acceleration, m s^{-2}
h	heat transfer coefficient, W m^{-2} K^{-1}
H	height, m, Fig. 1
K	constant
L	length scale, m
$\dot{m}$	mass flow rate, kg s^{-1}
$\dot{m}_{scale}$	mass flow rate scale, kg s^{-1}
N	number of riser tubes
q	heat transfer rate, W
Re	Reynolds number
r_2	acceleration factor, Eq. (34)
r_3	friction factor, Eq. (29)
r_4	gravitational factor, Eq. (23)
T_g	hot gas temperature, °C
T_{in}	inlet fluid temperature, °C
V	total volume, m^3
v_f	specific volume of saturated liquid, m^3/kg
v_{fg}	change of specific volume between phases, m^3/kg
v_g	specific volume of saturated vapor, m^3/kg
$V_{1,2}$	velocity, m s^{-1}
x	quality of liquid–vapor mixture

Greek symbols

ΔP	pressure drop, Pa
ΔP_f	friction pressure drop, Pa
ΔP_{acc}	acceleration pressure drop, Pa
λ	Lagrange multiplier
μ	dynamic viscosity, N s m^{-2}
ν	kinematic viscosity, m^2 s^{-1}
ξ	dimensionless group, Eq. (20)
ρ	density, kg/m^3
Φ	auxiliary function, Eq. (45)
Ψ	auxiliary function, Eq. (6)

Subscripts

c	cross-section
g	gas
max	maximum
min	minimum
opt	optimum
W	wall
1	downcomer
2	riser

Superscript

~	dimensionless

The circulation in the downcomer-riser-downcomer loop is driven by buoyancy effects, as the density of the liquid in the downcomer is greater than the density of the two-phase mixture in the riser. While the circulation continues because of the heating administered to the riser tubes, steam is collected from the upper plenum while make-up liquid is added to the same plenum.

2. Tube diameters

We begin with the pure fluid mechanics part of the problem, which is the maximization of steam generation rate per unit of flow volume. When the quality of the steam (x) produced by the riser is specified, the maximization of steam generation rate is the same as maximizing the circulation rate ($\dot{m}$) through the riser-downcomer loop.

The self-pumping effect [21–24] is due to the difference between the hydrostatic pressure sustained by the downcomer ($\rho_1 gH$) and the hydrostatic pressure sustained by the riser ($\rho_2 gH$), where $\rho_1 > \rho_2$, and H is the height of both columns. The driving pressure difference $(\rho_1 - \rho_2)gH$ is balanced by the pressure losses encountered by the fluid during its circulation,

$$(\rho_1 - \rho_2)gH = \Delta P_1 + \Delta P_2 \tag{1}$$

For orientation, we begin with a simple model in which the fluid in both columns is modeled as liquid with constant properties. The pressure drop due to flow friction along each column is

$$\Delta P_{1,2} = 4 f_{1,2} \frac{H}{D_{1,2}} \frac{1}{2} \rho_{1,2} V_{1,2}^2 \tag{2}$$

We model the flow as fully turbulent in the fully rough regime, i.e. with constant friction factor f in each column. Mass conservation requires that the mass flow rate $\dot{m}$ is the same in both columns,

$$\dot{m} = \rho_1 \frac{\pi}{4} D_1^2 V_1 = \rho_2 N \frac{\pi}{4} D_2^2 V_2 \tag{3}$$

By using Eq. (3) to eliminate V_1 and V_2, we rewrite Eq. (1) as a global flow resistance that depends on D_1 and D_2:

$$\frac{(\rho_1 - \rho_2)g}{(32/\pi^2)\dot{m}^2} = \frac{f_1/\rho_1}{D_1^5} + \frac{f_2/\rho_2}{N^2 D_2^5} \tag{4}$$

The two sizes, D_1 and D_2, vary subject to the total volume constraint

$$\frac{\pi}{4} D_1^2 H + N \frac{\pi}{4} D_2^2 H = V, \text{ constant} \tag{5a}$$

which means that

$$D_1^2 + N D_2^2 = \text{constant} \tag{5b}$$

The method of undetermined coefficients (or Lagrange multipliers) delivers the optimal D_1 and D_2 for which the global flow resistance (4) is minimal. The method consists of constructing a linear combination of the right-hand sides of Eqs. (4) and (5b)

$$\Psi = \frac{f_1/\rho_1}{D_1^5} + \frac{f_2/\rho_2}{N^2 D_2^5} + \lambda(D_1^2 + N D_2^2) \tag{6}$$

solving the two equations $\partial\Psi/\partial D_1 = 0$ and $\partial\Psi/\partial D_2 = 0$, and eliminating λ. The result is

$$\left(\frac{D_1}{D_2}\right)_{opt} = \left(N^3 \frac{f_1}{f_2} \frac{\rho_2}{\rho_1}\right)^{1/7} \tag{7}$$

The conclusion is that $(D_1/D_2)_{opt}$ varies as $N^{3/7}$, because f_1/f_2 and ρ_2/ρ_1 are two constants. To obtain the actual values of D_1 and D_2, we combine Eq. (7) with the total flow volume constraint (5a).

The minimized global flow resistance that corresponds to this design is obtained by combining Eqs. (4), (5a), (7):

$$\left[\frac{(\rho_1-\rho_2)g}{(32/\pi^2)\dot{m}^2}\right]_{\min}=\left(\frac{\pi H}{4V}\right)^{5/2}\frac{f_1}{\rho_1}\left[1+\left(\frac{f_2/\rho_2}{f_1/\rho_1}\right)^{2/7}N^{1/7}\right]^{7/2} \tag{8}$$

It is to be expected that f_2/ρ_2 will be greater than f_1/ρ_1, because the ρ_2 liquid is lighter (it has bubbles), and because turbulent two-phase flow is more resistive than single phase, ($f_1 < f_2$). If f_2/ρ_2 is much greater than f_1/ρ_1, then Eq. (8) becomes

$$\left[\frac{(\rho_1-\rho_2)g}{(32/\pi^2)\dot{m}^2}\right]_{\min}\cong\left(\frac{\pi H}{4V}\right)^{5/2}\left(\frac{f_2}{\rho_2}\right)N^{1/2} \tag{9}$$

and, in addition to Eq. (7), the following results hold:

$$D_{1,\mathrm{opt}}=\left(\frac{4V}{\pi H}\right)^{1/2}b^{-1/7}N^{-1/14} \tag{10}$$

$$D_{2,\mathrm{opt}}=\left(\frac{4V}{\pi H}\right)^{1/2}N^{-1/2} \tag{11}$$

where

$$b=\frac{f_2/\rho_2}{f_1/\rho_1}>1 \tag{12}$$

Note that both tube sizes decrease as N increases, but D_2 decreases much faster than D_1. The minimal flow resistance increases in proportion with the group $(H/V)^{5/2}(f_2/\rho_2)N^{1/2}$ and does not depend on (f_1/ρ_1). If V/H is the effective cross-sectional area (A_c) of all the tubes (downcomer and riser tubes), then the minimal flow resistance varies on $A_c^{-5/2}$. More attractive is to use a larger A_c and a smaller N, but in this limit the contact surface between the riser and the combustion gases that heat the ρ_2 stream is small. There is a tradeoff that leads to the optimal number of riser tubes N, and it comes from maximizing the heat transfer performance of the assembly.

3. Number of tubes

Consider next the rate of heat transfer (q) from hot gases to the ρ_2 liquid that flows through the N riser tubes. In a simple model, the fluid is single phase, the heat transfer conductance is accounted for by the overall heat transfer coefficient h, and the total tube contact surface is

$$A_W=\pi D_2 HN \tag{13}$$

The hot gases are considered isothermal at the temperature T_g. The temperature of the ρ_2 fluid at the inlets to the N tubes is T_{in}. The heat transfer rate q from T_g to the $\dot{m}$ stream is (Ref. [25], p. 319),

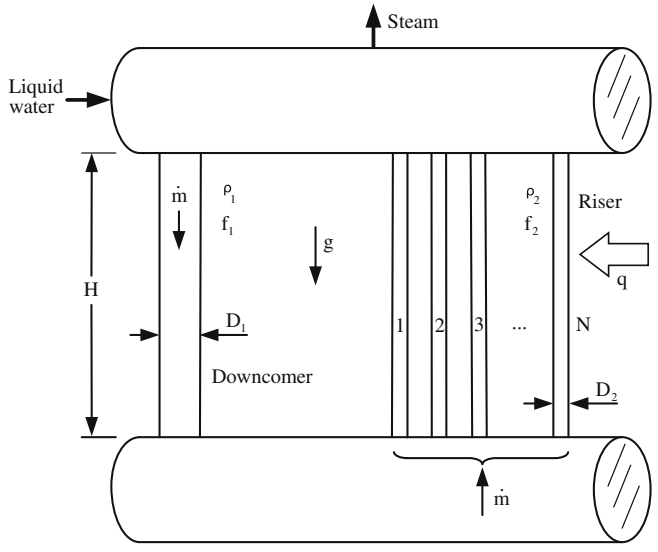

Fig. 1. Steam generator with self-pumping effect, downcomer and riser tubes.

$$q=\dot{m}c_P(T_g-T_{in})\left[1-\exp\left(-\frac{hA_W}{\dot{m}c_P}\right)\right] \tag{14}$$

Here all the parameters are known constants except $\dot{m}$ and A_W, which both depend on N. According to Eq. (9), the $\dot{m}(N)$ function is

$$\dot{m}=c_1N^{-1/4} \tag{15}$$

where c_1 is shorthand for the expression

$$c_1=\pi^{-1/4}\left[g(\rho_1-\rho_2)\frac{\rho_2}{f_2}\right]^{1/2}\left(\frac{V}{H}\right)^{5/4} \tag{16}$$

Eqs. (13) and (11) show that

$$A_W=c_2N^{1/2} \tag{17}$$

where

$$c_2=(4\pi VH)^{1/2} \tag{18}$$

Together, Eqs. (14)–(18) deliver q as a function of N, which can be summarized as

$$q=c_1c_P(T_g-T_{in})\left(\frac{c_2h}{c_1c_P}\right)^{1/3}\xi^{-1/3}(1-e^{-\xi}) \tag{19}$$

where

$$\xi=\frac{c_2h}{c_1c_P}N^{3/4} \tag{20}$$

The function $\xi^{-1/3}(1-e^{-\xi})$ reaches its maximum at $\xi_{\mathrm{opt}}=1.904$, which means that the optimal number of riser tubes is

$$N_{\mathrm{opt}}=\left(1.904\frac{c_1}{c_2}\frac{c_P}{h}\right)^{4/3} \tag{21}$$

Furthermore, because c_1 is proportional to $(V/H)^{5/4}$ and c_2 is proportional to $(VH)^{1/2}$, we conclude that N_{opt} is proportional to $V/H^{7/3}$, as follows

$$N_{\mathrm{opt}}=\left(1.904\frac{c_P}{2h}\right)^{4/3}\left[g(\rho_1-\rho_2)\frac{\rho_2}{f_2}\right]^{2/3}\frac{V}{\pi H^{7/3}} \tag{22}$$

Tall steam generators should have fewer riser tubes than short steam generators. The optimal number of riser tubes should be proportional to the total flow volume (downcomer and riser).

As a numerical example, consider a steam generator for a current large-scale power plant. Its global parameters are: $V=47\ \mathrm{m}^3$, $H=36\ \mathrm{m}$, $\rho_1=624\ \mathrm{kg/m}^3$, $\rho_2=518\ \mathrm{kg/m}^3$, $f_2=0.00475$, $c_P=7700\ \mathrm{J/kg\,K}$, and $h\sim10^4\ \mathrm{W/m}^2\,\mathrm{K}$. The fluid is water at $P=13.8\ \mathrm{MPa}$. Substituting these parameters in Eq. (22) we obtain $N_{\mathrm{opt}}=541$. In current 100 MW power plant designs the number of the designed riser tubes is approximately 400. The agreement is good in an order of magnitude sense. The discrepancy between 541 and 400 tubes can be attributed to the overall heat transfer coefficient h, the single phase flow assumption in the analysis, or to the fact that in practice N is not optimized. With the exception of h, all the data assumed in Eq. (22) are fixed as properties and physical dimensions that are known with certainty. Therefore, to evaluate the validity of the optimal number of the riser tubes Eq. (22), the overall heat transfer coefficient must be investigated and this means that a more accurate heat transfer model is required for a definitive constructal design.

4. Two-phase flow in the riser tubes

In Sections 2 and 3 we relied on simple models in order to demonstrate the opportunity for discovering from principle the main features of the flow architecture: the tube diameters and the number of riser tubes. In the second part of two-phase flow we rely on

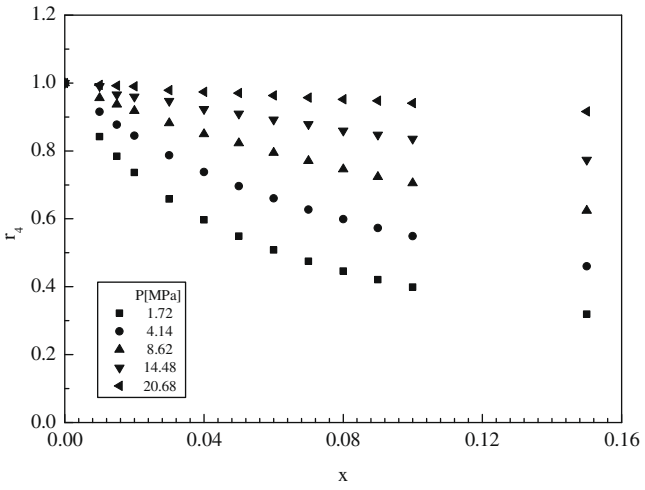

Fig. 2. The r_4 factor for two-phase mixture gravitational pressure drop [26].

more accurate models of two-phase flow in order to refine the calculation procedure and the features of the constructal architecture.

Consider the more realistic model where the flow in the riser tubes is two-phase. To start with, in Eq. (1) the density ρ_2 is replaced with by r_4/v_f

$$\left(\rho_1 - \frac{r_4}{v_f}\right)gH = \Delta P_1 + \Delta P_2 \tag{23}$$

where r_4 is the gravitational factor [26] for the two-phase liquid–steam mixture column, and v_f is the specific volume of saturated liquid. The gravitational factor r_4 accounts for the void slip effect on the density of liquid–steam in the vertical column, Fig. 2, where x is the quality of the two-phase mixture. The frictional pressure loss along the downcomer is, cf. Eq. (2),

$$\Delta P_1 = 4f_1\frac{H}{D_1}\frac{1}{2}\rho_1 V_1^2 \tag{24}$$

where V_1 is the mean water velocity in the downcomer,

$$V_1 = \frac{\dot{m}}{\rho_1(\pi/4)D_1^2} \tag{25}$$

and D_1 is the inner diameter of the downcomer column. The friction factor f_1 is a function of the downcomer Reynolds number

$$Re_1 = \frac{V_1 D_1}{\nu_1} = \frac{\dot{m}}{(\pi/4)D_1\mu_1} \tag{26}$$

and the roughness of the downcomer surface. This function is provided by the correlations displayed in the Moody chart [27]. In the present analysis we assume that the surface is smooth, and use a smooth-wall correlation proposed [28] for the range $2\times10^3 < Re_1 < 10^7$:

$$f_1(Re_1) = \frac{1}{4(1.82\log_{10}Re_1 - 1.64)^2} \tag{27}$$

The pressure loss along the riser tubes is due to two effects, friction (ΔP_f) and acceleration (ΔP_{acc}) [26]

$$\Delta P_2 = \Delta P_f + \Delta P_{acc} \tag{28}$$

The pressure drop due to friction in the two-phase flow is

$$\Delta P_f = 4f_2\frac{H}{D_2}\frac{v_f}{2}\left(\frac{\dot{m}}{A_2}\right)^2 r_3 \tag{29}$$

where D_2 is the inner diameter of one riser tube, r_3 is the dimensionless friction factor for two-phase flow [26] (see Fig. 3), and A_2 is the cross section area of all the riser tubes,

$$A_2 = N\frac{\pi D_2^2}{4} \tag{30}$$

In accordance with the model used for the downcomer, we also define the riser flow velocity, friction factor and Reynolds number:

$$V_2 = \frac{\dot{m}/N}{\rho_2(\pi/4)D_2^2} \tag{31}$$

$$f_2(Re_2) = \frac{1}{4(1.82\log_{10}Re_2 - 1.64)^2} \tag{32}$$

$$Re_2 = \frac{V_2 D_2}{\nu_2} = \frac{\dot{m}/N}{(\pi/4)D_2\mu_2} \tag{33}$$

The pressure drop due to acceleration in two-phase flow is

$$\Delta P_{acc} = v_f\left(\frac{\dot{m}}{A_2}\right)^2 r_2 \tag{34}$$

where r_2 is the dimensionless acceleration factor [26], shown here in Fig. 4. Substituting the pressure drop terms in Eq. (23), we obtain the global flow resistance equation for the self-pumping flow system:

$$\frac{g\pi^2\rho_1^2 H}{32\dot{m}^2}(1-r_4) = \frac{r_2}{2N^2D_2^4} + \frac{f_1 H}{D_1^5} + \frac{r_3 f_2 H}{N^2 D_2^5} \tag{35}$$

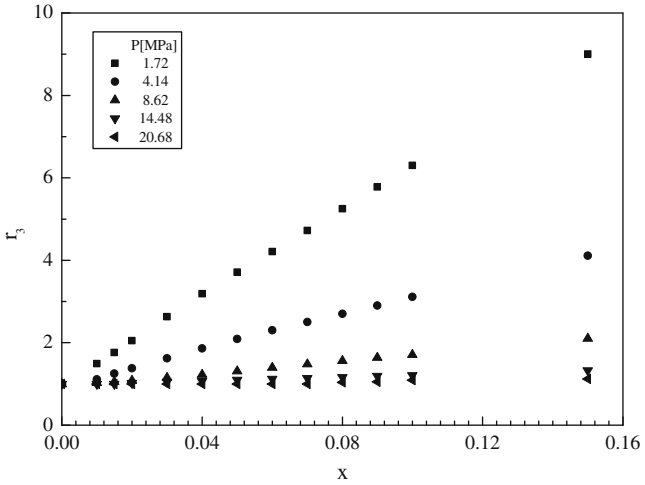

Fig. 3. The r_3 factor for two-phase mixture frictional pressure drop [26].

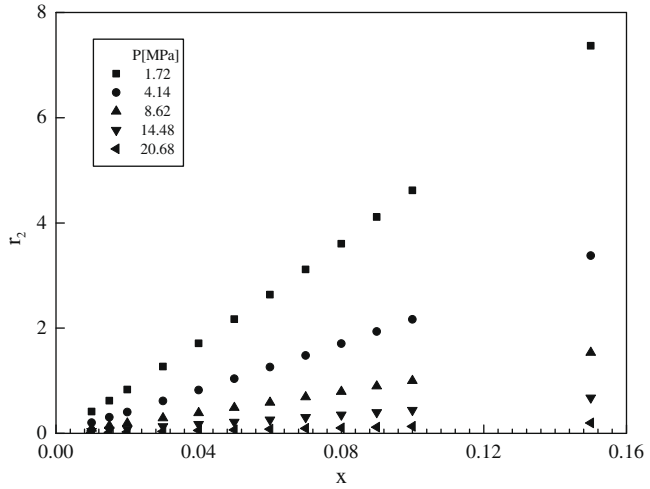

Fig. 4. The r_2 factor for two-phase mixture acceleration pressure drop [26].

The left side is a global flow resistance indicator, which in turbulent flow is essentially the driving pressure difference divided by $\dot{m}^2$. The constant volume constraint is shown in Eqs. (5a) and (5b). The length scale of the flow structure is indicated by Eq. (5a), where we set $D_{1,2} \sim L$:

$$L = \left(\frac{4V}{\pi H}\right)^{1/2} \tag{36}$$

From this length scale follow the dimensionless tube sizes

$$\tilde{D}_1 = \frac{D_1}{L}, \quad \tilde{D}_2 = \frac{D_2}{L} \tag{37}$$

and the dimensionless flow volume constraint:

$$\tilde{D}_1^2 + N\tilde{D}_2^2 = 1 \tag{38}$$

The scale of the mass flow rate ($\dot{m}_{\text{scale}}$) follows from Eq. (35), where we write $\dot{m} \sim \dot{m}_{\text{scale}}$ and $D_{1,2} \sim L$,

$$\frac{g\pi^2\rho_1^2}{32\dot{m}_{\text{scale}}^2} = \frac{f}{L^5} \tag{39}$$

therefore,

$$\dot{m}_{\text{scale}} = \rho_1 g^{1/2}\left(\frac{4V}{\pi H}\right)^{5/4} \tag{40}$$

$$\tilde{H} = \frac{H}{L}, \quad \tilde{m} = \frac{\dot{m}}{\dot{m}_{\text{scale}}} \tag{41}$$

The dimensionless version of Eq. (35) becomes

$$\frac{\pi^2}{32}\frac{\tilde{H}}{\tilde{m}^2}(1-r_4) = \frac{r_2}{2N^2\tilde{D}_2^4} + \frac{f_1\tilde{H}}{\tilde{D}_1^5} + \frac{r_3}{N^2}\frac{f_2\tilde{H}}{\tilde{D}_2^5} \tag{42}$$

where

$$Re_1 = \frac{B_1\tilde{m}}{\tilde{D}_1}, \quad Re_2 = \frac{B_2\tilde{m}}{N\tilde{D}_2} \tag{43}$$

$$B_1 = \frac{4}{\pi}\frac{g^{1/2}}{\nu_1}L^{3/2}, \quad B_2 = \frac{4}{\pi}\frac{g^{1/2}}{\nu_2}L^{3/2} \tag{44}$$

Two dimensions vary, $\tilde{D}_1$ and $\tilde{D}_2$, but in view of the volume constraint (38) only one parameter is free to vary, for example the ratio $\tilde{D}_1/\tilde{D}_2$. According to the method of Lagrange multipliers (Section 2), we form the linear combination of the right-hand sides of Eqs. (42) and (38),

$$\Phi = \frac{r_2}{2N^2\tilde{D}_2^4} + \frac{f_1\tilde{H}}{\tilde{D}_1^5} + \frac{r_3}{N^2}\frac{f_2\tilde{H}}{\tilde{D}_2^5} + \lambda(\tilde{D}_1^2 + N\tilde{D}_2^2) \tag{45}$$

and solve the system $\partial\Phi/\partial\tilde{D}_1 = 0$ and $\partial\Phi/\partial\tilde{D}_2 = 0$. After eliminating λ, we obtain

$$N^3\left(\frac{\tilde{D}_2}{\tilde{D}_1}\right)^7 = \frac{2r_2\tilde{D}_2}{5f_1\tilde{H}} + \frac{r_3 f_2}{f_1} \tag{46}$$

The second term dominates on the right-hand side of Eq. (46) when

$$\frac{\tilde{D}_2}{\tilde{H}} << \frac{5r_3}{2r_2}f_2 \tag{47}$$

and in this limit Eq. (46) delivers the optimal ratio of tube diameters

$$\left(\frac{\tilde{D}_1}{\tilde{D}_2}\right)_{\text{opt}} = \left(N^3\frac{f_1}{f_2 r_3}\right)^{1/7} \tag{48}$$

The assumption (47) is justified because the height is much greater than the diameter of the riser tubes ($D_2/H \sim 10^{-4}$), the factor r_3 is significantly greater than the acceleration factor r_2, and f_2 is of order 10^{-2} [26]. Even though r_2 approaches r_3 when $P < 5$ MPa and the liquid–vapor mixture quality (x) is greater than 0.1, the ratio $5r_3f_2/2r_2$ is of order 10^{-2}, i.e. much greater than the ratio D_2/H.

Eq. (48) resembles Eq. (7), which came from a much simpler model. The effect of two-phase flow in the riser is conveyed by r_3, which depends on pressure P and quality x [26]. In order to calculate the $\tilde{D}_1/\tilde{D}_2$ of Eq. (48) we need to account for the flow regime [Eqs. (27) and (32)] and the mass flow rate. The latter comes from the minimized flow resistance, which is obtained by combining Eqs. (48) and (38) with Eq. (42),

$$\left[\frac{\pi^2}{32}\frac{\tilde{H}}{\tilde{m}^2}(1-r_4)\right]_{\min} = \frac{r_2(K^2+N)^2}{2N^2} + \frac{f_1\tilde{H}(K^2+N)^{5/2}}{K^5} + \frac{r_3}{N^2}f_2\tilde{H}(K^2+N)^{5/2} \tag{49}$$

where $K = (N^3 f_1/f_2 r_3)^{1/7}$. The results presented in the next section are based on assuming the same global parameters as in Section 3, for example $V = 47\ \text{m}^3$ and $H = 36$ m. The resulting range for the mass flow rate is such that the Reynolds numbers calculated with Eqs. (26) and (33) vary in the ranges $1.9 \times 10^7 < Re_1 < 1.4 \times 10^8$ and $3 \times 10^5 < Re_2 < 1.2 \times 10^8$.

5. The effect of operating pressure

The results developed in the preceding section are sensitive to the pressure in the loop and the quality of the two-phase mixture

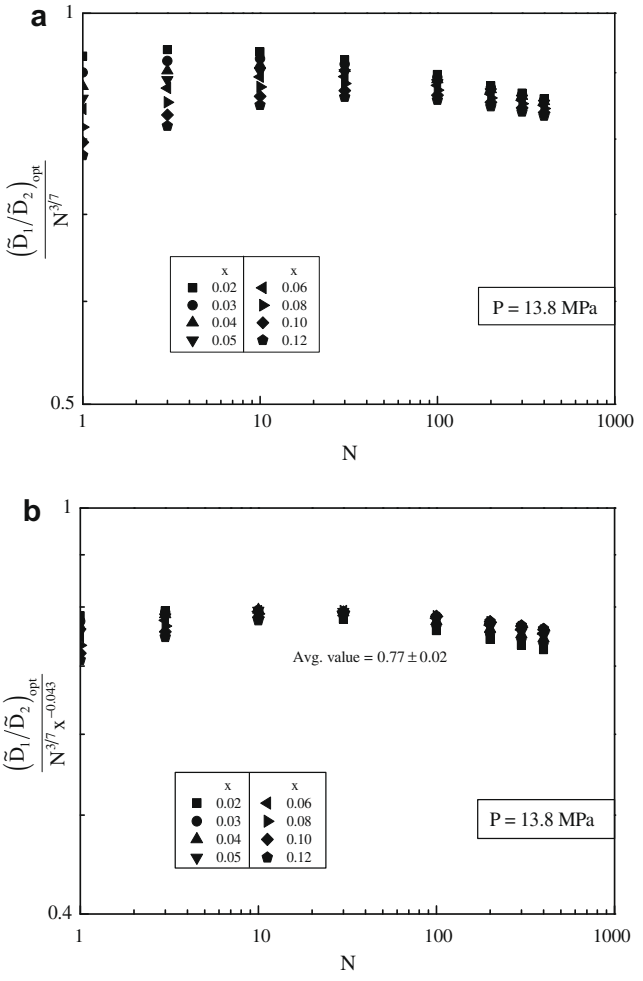

Fig. 5. (a) The effect of N and x on the optimal diameter ratio when 13.8 MPa; (b) optimal diameter ratio correlation.

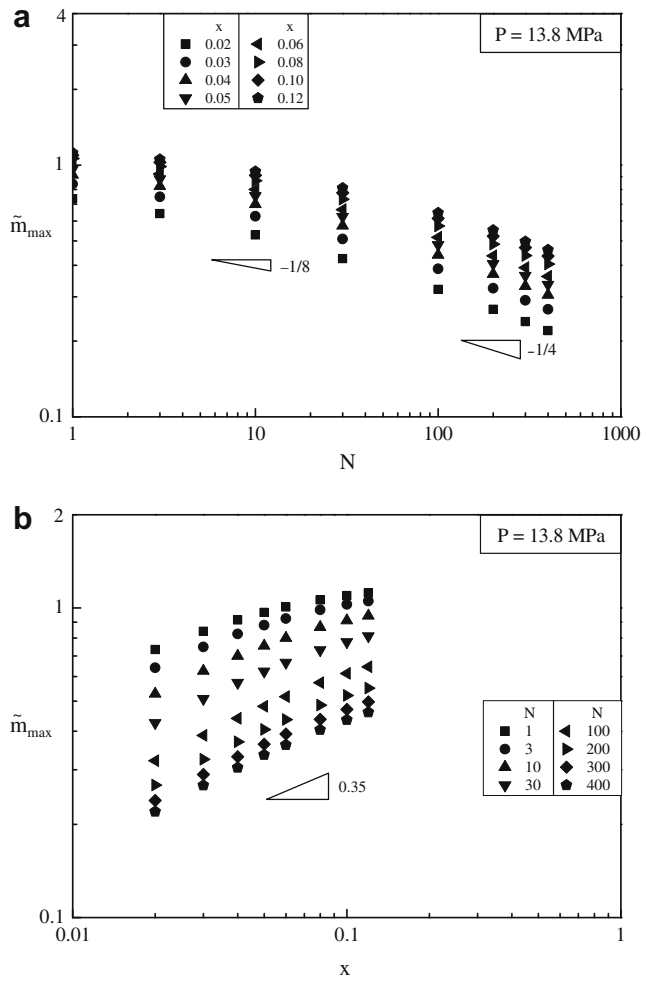

Fig. 6. (a) The effect of N on the dimensionless maximum mass flow rate when 13.8 MPa; (b) the effect of x on the dimensionless maximum mass flow rate.

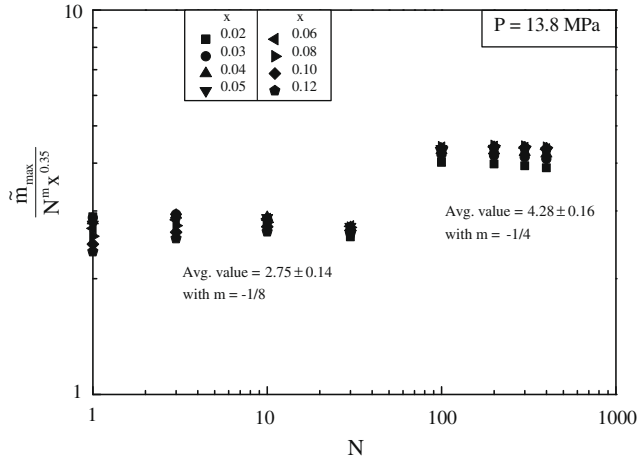

Fig. 7. Correlation of the dimensionless maximum mass flow rate for 13.8 MPa.

in the riser tubes. These effects are investigated systematically in Figs. 5–11, and can be anticipated based on the simple model of Section 2.

We begin with Fig. 5a, where we set $P = 13.8$ MPa and recognized [based Eq. (48)] that $(\tilde{D}_1/\tilde{D}_2)_{opt}$ should be proportional to $N^{3/7}$. Even though we plotted $(\tilde{D}_1/\tilde{D}_2)_{opt}/N^{3/7}$ on the ordinate, a

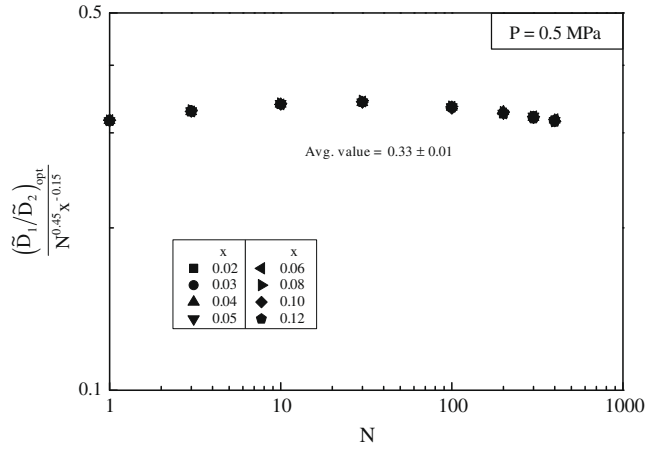

Fig. 8. Optimal diameter ratio correlation for 0.5 MPa.

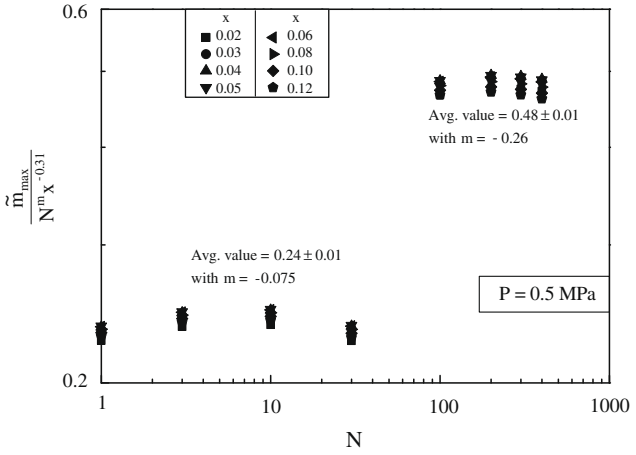

Fig. 9. Correlation of the dimensionless maximum mass flow rate for 0.5 MPa.

weak N effect continues to be present. Stronger is the effect of the quality x, which was given values in the range 0.02–0.12. The x effect is captured by the factor $x^{-0.043}$, which appears in the ordinate of Fig. 5b. The exponent −0.043 was determined by minimizing the scatter that is still visible in Fig. 5b. The conclusion is that for $P = 13.8$ MPa the optimal allocation of flow volume is represented by

$$\left(\frac{\tilde{D}_1}{\tilde{D}_2}\right)_{opt} = (0.77 \pm 0.02)N^{3/7}x^{-0.043} \tag{50}$$

The corresponding maximized mass flow rate $\tilde{m}_{max}$ is reported in Fig. 6a. The sensitivity of $\tilde{m}_{max}$ to N changes as N increases, namely from $\tilde{m}_{max} \sim N^{-1/8}$ to $\tilde{m}_{max} \sim N^{-1/4}$. Fig. 6b shows the effect of x, which is a rough proportionality between $\tilde{m}_{max}$ and $x^{0.35}$. Together, these power-law trends lead to the dimensionless correlations reported in Fig. 7, namely

$$\begin{aligned} \tilde{m}_{max} &= (2.75 \pm 0.14)N^{-1/8}x^{0.35}, \quad (N \le 50) \\ \tilde{m}_{max} &= (4.28 \pm 0.16)N^{-1/4}x^{0.35}, \quad (N \ge 50) \end{aligned} \tag{51}$$

The trends change somewhat when the pressure changes. Fig. 8 shows the $P = 0.5$ MPa equivalent of Fig. 5b. This time, instead of Eq. (50) the optimal ratio of diameters is correlated by

$$\left(\frac{\tilde{D}_1}{\tilde{D}_2}\right)_{opt} = (0.33 \pm 0.01)N^{0.45}x^{-0.15} \tag{52}$$

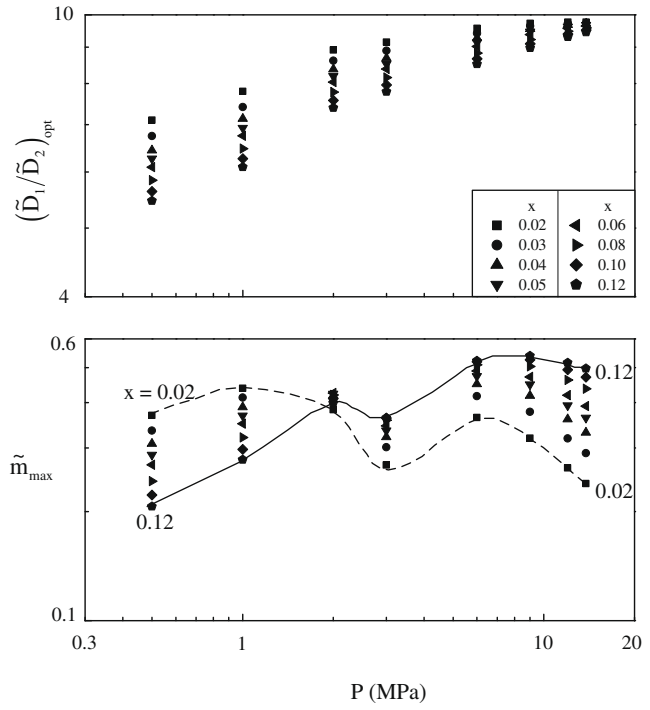

Fig. 10. The effect of pressure on the optimal diameter ratio and the dimensionless maximum mass flow rate.

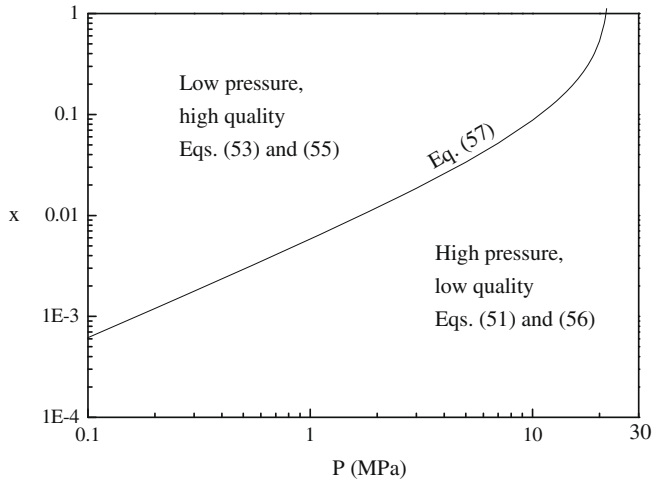

Fig. 11. The relationship $x(P)$ that serves as boundary between the domain of applicability of Eqs. (55) and (56).

Here the N exponent 0.45 is consistent with the N exponent in Eq. (48), namely 3/7 = 0.43. The maximized mass flow rate at P = 0.5 MPa is correlated in Fig. 9, as follows:

$$\begin{aligned}\tilde{m}_{max} &= (0.24 \pm 0.01) N^{-0.075} x^{-0.31}, \quad (N \le 50)\\ \tilde{m}_{max} &= (0.48 \pm 0.01) N^{-0.26} x^{-0.31}, \quad (N \ge 50)\end{aligned} \tag{53}$$

The effect of pressure is documented further in Fig. 10. As the pressure increases, the optimal diameter ratio $(\tilde{D}_1/\tilde{D}_2)_{opt}$ increases for every value of x. The maximum mass flow rate exhibits a more complicated behavior. At low pressures, the maximum mass flow rate decreases as the quality increases. At pressures above 2 MPa, the maximum mass flow rate increases with quality.

This reversal in how $\tilde{m}_{max}$ depends on x is explained by the analytical solution developed in Section 2. If we take the mass flow rate maximized in Eq. (9) and nondimensionalize it in accordance with Eqs. (40) and (41) we obtain

$$\tilde{m}_{max} = 2^{-5/2} \pi f_2^{-1/2} N^{-1/4} \frac{(x v_f v_{fg})^{1/2}}{v_f + x v_{fg}} \tag{54}$$

where we replaced ρ_1^{-1} with the specific volume of saturated liquid, $v_f(P)$. We also replaced ρ_2^{-1} with $(v_f + x v_{fg})$, where $v_{fg} = v_g - v_f$ and $v_g(P)$ is the specific volume of saturated vapor. In the limit $x \ll 1$, the denominator $(v_f + x v_{fg})$ depends on pressure in two ways. When the pressure is sufficiently low, v_f is negligible relative to $x v_{fg}$ and Eq. (54) approaches

$$\tilde{m}_{max,low\ P} \cong \left[2^{-5/2} \pi f_2^{-1/2} \left(\frac{v_f}{v_{fg}} \right)^{1/2} \right] N^{-1/4} x^{-1/2} \tag{55}$$

As P approaches the critical pressure, the difference between v_g and v_f disappears and $x v_{fg}$ is negligible relative to v_f. In this limit Eq. (54) approaches

$$\tilde{m}_{max,high\ P} \cong \left[2^{-5/2} \pi f_2^{-1/2} \left(\frac{v_{fg}}{v_f} \right)^{1/2} \right] N^{-1/4} x^{1/2} \tag{56}$$

Eqs. (55) and (56) confirm qualitatively the dependence of $\tilde{m}_{max}$ on N and x, which was correlated as Eqs. (53) and (51), respectively. See the correlations reported for $N \ge 50$. Dividing Eqs. (55) and (56), we see that the transition from one behavior to the other occurs when the pressure P is such that

$$\frac{v_f(P)}{v_{fg}(P)} \cong x \tag{57}$$

This relationship between x and P has been plotted for water in Fig. 11, and it divides the $x - P$ domain into the two subdomains in which Eqs. (51) and (53) apply.

In closing, we relaxed the assumption that the height H is fixed, and investigated the effect of H on the main features of the design, $(\tilde{D}_1/\tilde{D}_2)_{opt}$ and $\tilde{m}_{max}$. Fig. 12 shows that these features are insensitive to H. This can be also shown analytically, because, when the assumption (47) is valid, $\tilde{H}$ drops out from Eq. (42), leaving only

$$\frac{\pi^2}{32 \tilde{m}^2} (1 - r_4) = \frac{f_1}{\tilde{D}_1^5} + \frac{r_3}{N^2} \frac{f_2}{\tilde{D}_2^5} \tag{58}$$

6. Conclusions

The main conclusion is that it is possible to derive the main features of an engineering flow component from the free search for

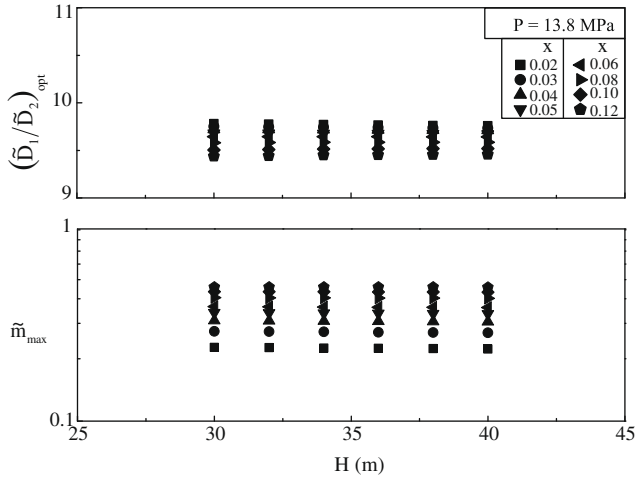

Fig. 12. The effect of H on the optimal diameter ratio and the dimensionless maximum mass flow rate when 13.8 MPa.

flow configuration when the global size is constrained. Here we illustrated the constructal design method [2] by focusing an the steam generator, for which we derived the dimensions of the tubes, the number of riser tubes, and the circulation flow rate (and the related steam production rate) – all for specified global size, flow volume V and height H.

The added benefit of these results is the size effect (V,H), i.e. the *scaling*. This means that the designer can predict how the drawing *morphs* when the allotted size changes. Scaling up and scaling down are now possible because the principle of generation of flow configuration is in hand.

Another practical aspect that is consistent with the present results is that engineers have long classified steam generators according to pressure. In other words, the pressure is an essential factor in the design of the steam generator. The constructal design developed in this paper sheds light on the effect of pressures on the main geometric characteristics of steam generator architecture. The results obtained with the two-phase flow model show that the optimal configuration of the steam generator is pressure dependent because the quality depends on the pressure and is a crucial factor in minimizing the global flow resistance. This observation is consistent with current designs of steam generators, which have evolved based on the "design, build and test method" over a long time. The designs show different configurations, one for each pressure.

What we showed here for the design of the steam generator can and should be extended to the other components of the power plant. Each owes its thermodynamic imperfection to its finite size and flow configuration. The finite size cannot be changed, at least at the component – concept stage. The flow configuration can be changed, and this is the path to discovering less and less imperfect components for a given size.

At the power plant level, the many components conceptualized in this manner can be assembled into one "construct" that relies on the fixed sizes of the many. It is at this level that scaling yields benefit, by allowing tradeoffs between the size of one component against the size of another. All such tradeoffs lead to the distribution of "sizes" over the entire installation, with the global objective of improving the global efficiency of the power plant. The distributing of sizes is leading the design in the same direction as the more established methods of distributing (balancing) the destruction of exergy, or generation of entropy [3,29–31].

Acknowledgement

This research was supported by Doosan Heavy Industries & Construction Co., Ltd., Changwon, South Korea.

References

[1] A. Bejan, S. Lorente, Constructal theory of generation of configuration in nature and engineering, J. Appl. Phys. 100 (2006) 041301.
[2] A. Bejan, S. Lorente, Design with Constructal Theory, Wiley, Hoboken, NJ, 2008.
[3] A. Bejan, Advanced Engineering Thermodynamics, second ed., Wiley, New York, 1997.
[4] A. Bejan, Shape and Structure, from Engineering to Nature, Cambridge University Press, Cambridge, UK, 2000.
[5] A.H. Reis, Constructal theory: from engineering to physics, and how flow systems develop shape and structure, Appl. Mech. Rev. 59 (2006) 269–282.
[6] G. Hernandez, J.K. Allen, F. Mistree, Platform design for customizable products as a problem of access in a geometric space, Eng. Optimiz. 35 (2003) 229–254.
[7] Y. Chen, P. Cheng, Heat transfer and pressure drop in fractal tree-like microchannel nets, Int. J. Heat Mass Transfer 45 (2002) 2643–2648.
[8] D.V. Pence, Reduced pumping power and wall temperature in microchannel heat sinks with fractal-like branching channel networks, Microscale Thermophys. Eng. 6 (2002) 319–330.
[9] A.H. Reis, A.F. Miguel, M. Aydin, Constructal theory of flow architecture of the lungs, J. Med. Phys. 31 (2004) 1135–1140.
[10] S.M. Senn, D. Poulikakos, Laminar mixing, heat transfer, and pressure drop in tree like microchannel nets and their application for thermal management in polymer electrolyte fuel cells, J. Power Sources 130 (2004) 178–191.
[11] S.M. Senn, D. Poulikakos, Tree network channels as fluid distributors constructing double-staircase polymer electrolyte fuel cells, J. Appl. Phys. 96 (2004) 842–852.
[12] F. Lundell, B. Thonon, J.A. Gruss, Constructal networks for efficient cooling/heating, Second Conference on Microchannels and Minichannels, Rochester, NY, 2004.
[13] V.A.P. Raja, T. Basak, S.K. Das, Thermal performance of multi-block heat exchanger designed on the basis of Bejan's constructal theory, Int. J. Heat Mass Transfer 51 (2008) 3582–3594.
[14] M. Lallemand, F. Ayela, M. Favre-Marinet, A. Gruss, D. Maillet, P. Marty, H. Peerhossaini, L. Tadrist, Thermal transfer in microchannels: applications to micro-exchangers, French Congress on Thermics, SFT 2005, Reims, 30 May–2 June 2005.
[15] N. Kockmann, T. Kiefer, M. Engler, P. Woias, Channel networks for optimal heat transfer and high throughput mixers, ECI International Conference on Heat Transfer and Fluid Flow in Microscale, Castelvecchio Pascoli, Italy, 2005.
[16] Y.S. Muzychka, Constructal design of forced convection cooled microchannel heat sinks and heat exchangers, Int. J. Heat Mass Transfer 48 (2005) 3119–3127.
[17] Y.S. Muzychka, Constructal multi-scale design of compact micro-tube heat sinks and heat exchangers, Int. J. Therm. Sci. 46 (2007) 245–252.
[18] X.-Q. Wang, A.S. Mujumdar, C. Yap, Numerical analysis of blockage and optimization of heat transfer performance of fractal-like microchannel nets, J. Electron. Packag. 128 (2006) 38–45.
[19] S.C. Stultz, J.B. Kitto (Eds.), Babcock & Wilcox STEAM its generation and use, Babcock & Wilcox, 2005.
[20] J.G. Singer (Ed.), Combustion Engineering: A Reference Book on Fuel Burning and Steam Generation, Revised Edition, Combustion Engineering, Inc., New York, 1991.
[21] M.J. Lighthill, Theoretical considerations on free convection in tubes, Quart. J. Mech. Appl. Math. 6 (1953) 398–439.
[22] B.W. Martin, Free convection in an open thermosyphon with special reference to turbulent flow, Proc. Roy. Soc. A230 (1955) 502–530.
[23] B.W. Martin, Free convection heat transfer in the inclined open thermosyphon, Proc. Inst. Mech. Eng. 173 (1959) 761–778.
[24] B.W. Martin, H. Cohen, Heat transfer by free convection in an open thermosyphon tube, B. J. Appl. Phys. 5 (1954) 91–95.
[25] A. Bejan, Heat Transfer, Wiley, New York, 1993.
[26] J.R.S. Thom, Prediction of pressure drop during forced circulation boiling of water, J. Heat Mass Transfer 7 (1964) 709–724.
[27] L.F. Moody, Friction factors for pipe flow, Trans. ASME 66 (1944) 671–684.
[28] J.P. Holman, Heat Transfer, fifth ed., McGraw-Hill, 1981.
[29] M. Moran, A Guide to Efficient Energy Use, second ed., ASME Press, New York, 1989.
[30] E. Sciubba, R. Melli, Artificial Intelligence in Thermal Systems Design: Concepts and Applications, Nova Science Publishers, New York, 1998.
[31] A. Bejan, Entropy Generation through Heat and Fluid Flow, Wiley, New York, 1982.